Deep Learning Classification of Blackcurrant Genotypes by Ploidy Levels on Stomata Microscopic Images

Aleksandra Konopka[1][0000−0003−1730−5866], Karol Struniawski[1][0000−0002−4574−2986], Ryszard Kozera[1,2][0000−0002−2907−8632], Luciano Ortenzi[3][0000−0002−1245−8882], Agnieszka Marasek-Ciołakowska[4][0000−0001−9349−2566] and Aleksandra Machlańska[4][0000−0003−3582−1573]

[1] Institute of Information Technology,
Warsaw University of Life Sciences - SGGW,
ul. Nowoursynowska 159, 02-776 Warsaw, Poland
{aleksandra_konopka, karol_struniawski, ryszard_kozera}@sggw.edu.pl
[2] School of Physics, Mathematics and Computing,
The University of Western Australia,
35 Stirling Highway, Crawley, WA 6009, Perth, Australia
ryszard.kozera@uwa.edu.au
[3] Department of Computer Science,
Sapienza University of Rome,
Viale Regina Elena, 295, 00161, Rome, Italy
luciano.ortenzi@unitus.it
[4] Department of Applied Biology,
The National Institute of Horticultural Research,
Konstytucji 3 Maja 1/3, 96-100 Skierniewice, Poland
{agnieszka.marasek, aleksandra.machlanska}@inhort.pl

Abstract. Polyploidy, the variation in chromosome sets within plants, influences stomata size and density, making stomata analysis a valuable method for determining ploidy levels. Traditional microscopic analysis, nevertheless, is often labor-intensive and complex. This study explores the use of artificial intelligence for the automated classification of plant ploidy levels from stomata images, presenting a novel approach in this field. Experiments were conducted on three blackcurrant genotypes: diploid, triploid and tetraploid. Deep learning techniques were employed for stomata segmentation and classification, with performance compared to traditional machine learning algorithms, including K-Nearest Neighbors, Support Vector Machine, Random Forest and Multi-Layer Perceptron. To mitigate the impact of color variations that could lead to inflated accuracy, multiple datasets were processed to reduce the influence of color. Classification was performed not only on whole images but

[1] This work was partly supported by Polish Ministry of Science and Higher Education through statutory funds of The National Institute of Horticultural Research, Skierniewice, Poland (Grant ZBS/7/2021)

ICCS Camera Ready Version 2025
To cite this paper please use the final published version:
DOI: 10.1007/978-3-031-97564-6_11

also on subimages containing individual stomata instances, detected using the YOLOv8 algorithm. A majority voting approach was applied to classify the entire image based on subimage classifications. ResNet152v2 achieved the highest accuracy of 0.973 on color images, although accuracy declined when the influence of color was minimized. These results underscore the significant role of color in model performance and highlight the challenges associated with achieving reliable and robust classification.

Keywords: stomata, microscopic image classification, machine learning, deep learning, Residual Neural Networks, YOLO algorithm

1 Introduction

Stomata are microscopic pores found in the epidermal layers of plant leaves and other aerial tissues [21]. These pores are regulated by two specialized cells that control their opening and closing. The stomata play a crucial role in regulating the exchange of gases, including CO_2 and in controlling factors such as light intensity and humidity [5]. These factors can influence the visual characteristics of stomata. Additionally, stomata traits may also be affected by the application of biofertilizers, making the analysis of stomata cells a valuable method for assessing the effectiveness of biofertilizers [2, 32]. Structurally, stomata form an elliptical shape. Polyploidy, which refers to the number of chromosome sets in a plant, can be determined through the microscopic analysis of stomata characteristics. Both the size and density of stomata are influenced by polyploidy [35]. However, the process of analyzing stomata images to assess polyploidy can be time-consuming and complex. To address this challenge, the application of artificial intelligence (AI) has been proposed in this paper. Although AI is successfully applied to microscopic images of stomata for tasks such as segmentation [19], measurement [27] and counting [9], to the best of our knowledge, it has not yet been used for the automated classification of plant ploidy level based on stomata images.

In this study, experiments were conducted on three classes of blackcurrant genotypes, each distinguished by their ploidy level: diploid, triploid and tetraploid. The research faced several challenges, primarily because stomata characteristics are influenced by environmental factors [6]. Additionally, the color of the plant, as observed in microscopic images, is also affected by environmental conditions, further complicating the analysis. As a result, it is essential to ensure that each ploidy class is represented under similar environmental conditions. One challenge that arose was the variation in image color, which had the potential to artificially inflate accuracy (ACC) rates. To mitigate this, attention was concentrated on the shape of the stomata, and the impact of color was minimized to the greatest extent possible.

Due to subtle variations in brightness and color across the images, multiple datasets were generated as preprocessed versions of the raw dataset, enabling the evaluation of various analytical approaches. The analysis aimed to determine whether better classification results could be obtained by analyzing the entire image, considering all components and details of the leaf structure for

ICCS Camera Ready Version 2025
To cite this paper please use the final published version:
DOI: 10.1007/978-3-031-97564-6_11

each ploidy. Alternatively, it was explored whether focusing solely on the stomata cells would yield better outcomes. Furthermore, to reduce the influence of color on the classification results, several datasets characterized by different color spaces and channel configurations were examined in this paper.

In the latter, deep learning techniques were employed for the segmentation task to accurately identify stomata objects. For the classification task, deep learning models were applied and their performance was compared against traditional machine learning algorithms. Finally, majority voting (MV) [29] was employed on subimages to investigate whether classifying individual stomata objects, followed by MV, could improve the overall classification accuracy.

2 Materials

The experiment was carried out in the Experimental Pomological Orchard in Skierniewice, central Poland, belonging to the National Institute of Horticultural Research. Plants of blackcurrant (*Ribes nigrum* L.) were grown under natural light in 50 L pots filled with a mixture of peat substrate and soil at a ratio of 1:1. Water potential in the growing medium was maintained at a level (−) 10 kPa. The moisture content of the growing medium were monitored with dielectric probes (TEROS-12, METER, USA). Plants were maintained according to standard agrotechnical measures for the blackcurrant. Leaves were sampled for photo documentation at the end of a vegetation season from the 5th to the 25th of September 2024.

The dataset utilized in this research comprises three classes of blackcurrant genotypes distinguished by their chromosome counts: diploid ($2n = 2x = 16$) cultivar (class 0), triploid ($2n = 3x = 24$) cultivar (class 1) and tetraploid ($2n = 4x = 32$) clone (class 2) (see Figure 1). Class 0 includes 252 images of the 'Gofert' cultivar and 252 images of the 'Polares' cultivar. Class 1 contains 502 images of the triploid 'Dlinnokistnaja' cultivar, while class 2 consists of 251 images of the autotetraploid clone of 'Gofert' cultivar and 250 images of the 'Polares' cultivar obtained by in vitro poliyploidyzation [23]. All images were captured using the VHX-7000N KEYENCE digital microscope, ensuring high-quality imaging suitable for detailed analysis.

3 Methods

This work focuses on comparing classical artificial intelligence methods with approaches based on deep neural networks. Deep learning techniques were applied in this research to both image classification and segmentation tasks. The following subsections provide a detailed description of the selected deep learning methods.

3.1 Convolutional Neural Networks

This research leverages Convolutional Neural Networks (CNNs) [31] a class of deep learning models applied to tasks related with image processing and com-

ICCS Camera Ready Version 2025
To cite this paper please use the final published version:
DOI: 10.1007/978-3-031-97564-6_11

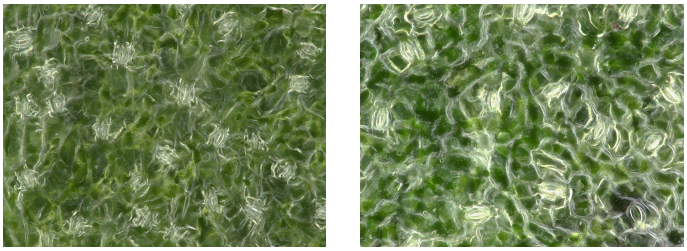

(a) (b)

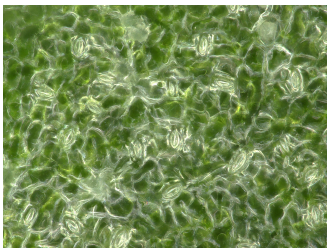

(c)

Fig. 1: Exemplary images of diploid (a), triploid (b) and tetraploid (c) genotypes from the raw dataset.

puter vision. CNNs, are widely recognized not only for their ability to perform classification, regression, object detection, segmentation task on input data [7] but also for their capacity to automatically extract relevant features. The image, which serves as the input to the CNN, undergoes processing through various network layers that iteratively extract features [10].

The term convolution in CNN refers to the convolution layer, a fundamental component responsible for performing convolution operation [8]. This procedure involves processing the input image with a filter, which is designed to emphasize specific aspects of the image, such as edges or patterns [15]. These filters are learned during training, allowing the network to identify features critical for the task at hand.

Another essential component of CNN is the pooling layer, which serves to distill the most significant information while discarding irrelevant details. The pooling operation reduces the spatial dimensions of the data, resulting in computational efficiency and mitigating resource constraints without sacrificing performance [33].

The convolution and pooling, along with other specialized layers, process the input image, transforming it into a feature vector. This vector serves as the input to the classification stage, typically implemented as a fully connected neural network - commonly referred to as a Multi-Layer Perceptron (MLP) [1]. This final stage performs classification or regression, depending on the specific task under consideration.

ICCS Camera Ready Version 2025
To cite this paper please use the final published version:
DOI: 10.1007/978-3-031-97564-6_11

Residual Neural Networks (ResNets) [26] are a specialized type of Convolutional Neural Networks created in 2016 [12] that were employed in this research for the classification task. A key architectural feature of ResNets is their ability to learn based on residual errors, utilizing skip connections to mitigate the vanishing gradient problem [28]. These networks have various versions, differing in the number of convolutional blocks and the arrangement of layers [17]. In this study, the ResNet50v2 and ResNet152v2 architectures [13] are considered.

3.2 YOLO

Convolutional Neural Networks form a core component of the YOLO (You Only Look Once) algorithm [24], a highly efficient and versatile deep learning framework. YOLO is widely utilized for tasks such as classification, object detection and instance segmentation. In this study, YOLO is employed to segment stomata in images.

YOLO is renowned for its speed and capability to detect multiple objects in a single pass [3]. The algorithm processes input data, typically images, by first scaling them to a predefined size. The scaled image is then divided into a grid structure, where each grid cell is responsible for detecting objects whose centers fall within that specific cell [4]. A CNN is then applied to extract features and detect objects within each grid cell.

The output of the CNN provides essential information, including the probability of an object's presence, the x and y coordinates of the object's center, its width and height, and a one-hot encoded vector representing the object's class [24]. Predicted bounding boxes are evaluated using the Intersection over Union metric, which measures the overlap between predefined bounding boxes for the target objects and those predicted by the model [34].

In the post-processing stage, the algorithm refines the detection results. First, the most probable object detections are retained and overlapping bounding boxes identifying the same object are eliminated using the Non-Maximum Suppression algorithm [25]. This step ensures that redundant boxes corresponding to multiple anchors in a single grid cell are removed. The final output of the YOLO algorithm is a list of detected objects.

The YOLO algorithm was originally introduced in 2015 and subsequent versions are developed to enhance its performance.

4 Experiments and results

The experiments were conducted in multiple stages using both the raw and processed versions of the dataset. Subimages containing individual stomata were extracted for analysis. The primary objective of this study was to evaluate and compare the classification accuracy of deep learning algorithms against traditional machine learning techniques. The latter presents classification outcomes for scenarios where the raw dataset, including color information, is used and other where the influence of color is minimized to focus exclusively on the shape

ICCS Camera Ready Version 2025
To cite this paper please use the final published version:
DOI: 10.1007/978-3-031-97564-6_11

of the stomata objects. The computations were performed using the Python programming language.

4.1 Image Segmentation

To identify stomata cells, the YOLOv8 algorithm was applied. This version of YOLO was chosen because its output is a precise segmentation mask that covers the area of the searched object, rather than a bounding box. For this segmentation task, the algorithm was trained on 70 images and validated on 30 images of tetraploid 'Polares' cultivar, which were manually segmented. The dataset used for training included images of blackcurrant subjected to varying water conditions (50 images under high irrigation and 50 images under low irrigation). This variation in water availability was introduced to ensure that the YOLO algorithm could learn to detect stomata cells of all sizes, as the size of the stomata changes depending on water availability.

The YOLOv8 model, using the *yolov8n-seg.pt* [14] configuration, was trained for 500 epochs. The image size was set to 2000 $\times$ 2000 pixels and a batch size of 5. To reduce computation time, the number of points in the labels used as input to the YOLO algorithm was reduced by a factor of 4 compared to those created by manual segmentation. The output of YOLO algorithm is a list of stomata object labels. Based on the coordinates of labels the stomata instances were identified which allowed creation of binary masks - white area represents stomata objects and black area is the remaining part of the image.

4.2 Preparation of various datasets

Due to variations in sample color, computations were performed on multiple datasets to reduce impact of color on classification accuracy. The first analyzed dataset was included raw images curated by biology experts. Additional 9 datasets were derived from this original dataset, incorporating modifications to minimize the influence of sample color. Figure 2 demonstrates a noticeable reduction in color variation across the selected color channels among the three classes. This is demonstrated through a comparative analysis of the mean green component in the RGB and grayscale image with the mean hue (H) component in the HSV color space and the mean value (V) component in the histogram-equalized HSV. The following datasets were considered (see Figure 3):

1. *Images* - unmodified raw images in the RGB color space.
2. *Grayscale images* - the *Images* converted to grayscale.
3. *HSV images - H* - the hue component of *Images* in the HSV color space.
4. *HSV images - V equalized* - the value component of *Images* in the HSV color space, with histogram equalization applied.
5. *Image masks* - binary masks of images.
6. *Subimages* - containing a single stoma extracted from the original images.
7. *Subimages black background* - *Subimages* with the background set to black (only the stoma object retains color).

ICCS Camera Ready Version 2025
To cite this paper please use the final published version:
DOI: 10.1007/978-3-031-97564-6_11

8. *Subimages grayscale* - *Subimages* converted to grayscale.
9. *Subimages grayscale black background* - *Subimages* converted to grayscale with the background set to black.
10. *Subimage masks* - binary masks of *Subimages*.

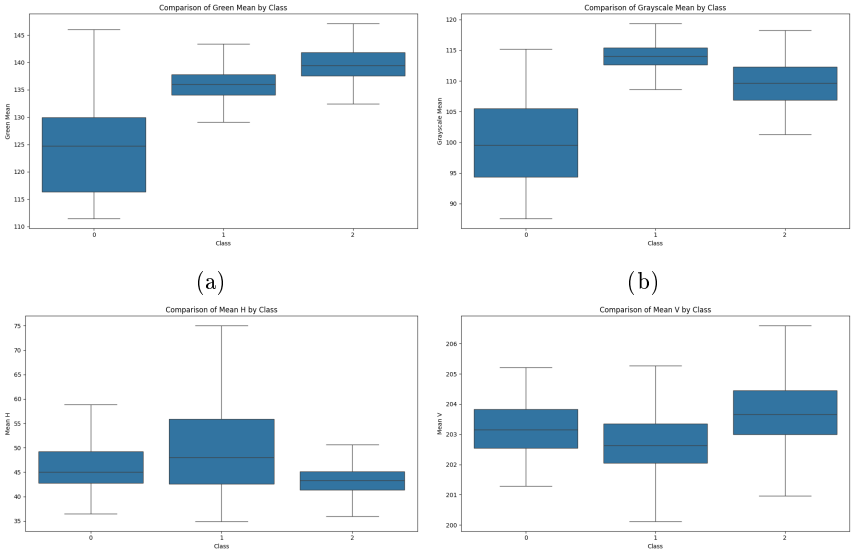

Fig. 2: The boxplots of mean values for three classes (0 - diploid, 1 - triploid, 2 - tetraploid) across selected channels: green from RGB (a), grayscale (b), hue from HSV (c) and equalized value from HSV (d).

Datasets 1–5 were derived from entire microscopic images, while datasets 6–10 were based on subimages. These subimages, measuring 224×224 pixels, were extracted with a single stoma centrally positioned within each image.

4.3 Classification with Residual Neural Networks

All 10 datasets were used as input to ResNet50v2 and ResNet152v2 models which were configured with the following parameter values. Each dataset was split into training, validation and test sets in a 7:2:1 ratio. The models were fine-tuned from ImageNet [17], starting from the layer *conv5_block1_1_conv*. The applied pooling method was average pooling. The classification part of the network included the following layers: a dense layer with 512 neurons and ReLU activation function, followed by a dropout layer with a rate of 0.3, another dense layer with 512 neurons and ReLU activation function, an additional dropout

ICCS Camera Ready Version 2025
To cite this paper please use the final published version:
DOI: 10.1007/978-3-031-97564-6_11

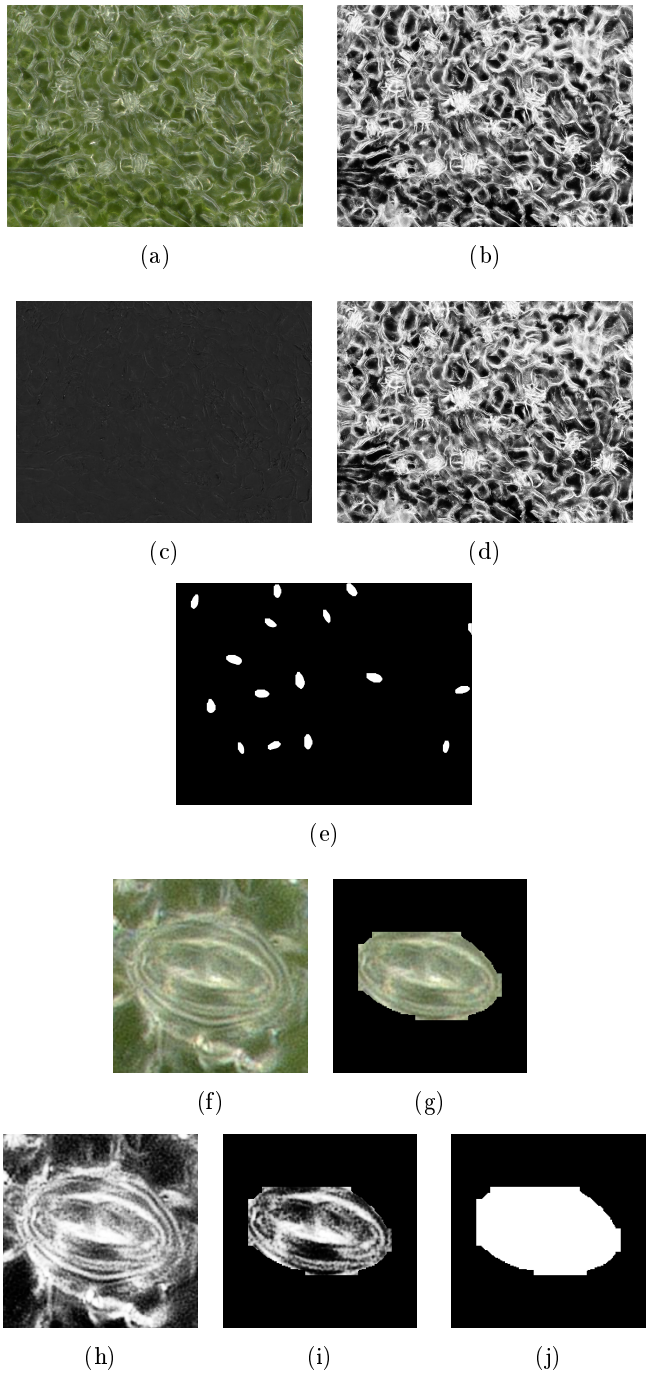

Fig. 3: Exemplary images from datasets 1–10, corresponding to subfigures (a–j), representing class 0 - diploid.

ICCS Camera Ready Version 2025
To cite this paper please use the final published version:
DOI: 10.1007/978-3-031-97564-6_11

layer and a final dense layer with a softmax activation function. The Adam optimizer was used with a learning rate of 0.01. An early stopping mechanism was implemented with a patience of 50 epochs, with a maximum of 1000 epochs and a batch size of 32. Table 1 presents accuracy values ranging from 0.606 for the *HSV images - H* dataset using ResNet50v2 to 0.973 for the *Images* dataset with ResNet152v2. For the *Image masks* dataset, ResNet50v2 achieved an accuracy of 0.787, while ResNet152v2 yielded an accuracy of 0.618 on the *Subimage masks* dataset.

Furthermore, datasets 6–10 were also subjected to a majority voting approach. Each subimage was classified into one of three classes. Subsequently, the image from which the subimage was extracted was assigned to the class that received the majority of classifications from its constituent subimages. The application of MV on subimages achieved a maximum accuracy of 0.96 with ResNet152v2 on the *Subimages* dataset. In contrast, for the *Subimage masks* dataset, MV with ResNet152v2 yielded an accuracy of 0.624 (see Table 1).

Dataset		**ResNet50v2**		**ResNet152v2**	
		no MV	*MV*	*no MV*	*MV*
1	*Images*	0.953	-	0.973	-
2	*Grayscale images*	0.953	-	0.88	-
3	*HSV images - H*	0.606	-	0.636	-
4	*HSV images - V equalized*	0.62	-	0.63	-
5	*Image masks*	0.787	-	0.68	-
6	*Subimages*	0.856	0.913	0.866	0.96
7	*Subimages black background*	0.68	0.765	0.759	0.765
8	*Subimages grayscale*	0.78	0.839	0.815	0.9
9	*Subimages grayscale black background*	0.783	0.859	0.782	0.9
10	*Subimage masks*	0.607	0.577	0.618	0.624

Table 1: Classification accuracy of stomata images on 10 different datasets applying Residual Neural Networks with majority voting applied - *MV* or without majority voting - *no MV*.

4.4 Classification with classical machine learning methods

In this study, the performance of ResNets was compared to classical machine learning techniques [16]. The dataset utilized in this comparison consisted of *Image masks*, which represent the shapes of stomata instances without relying on color information. For each image, features were manually extracted for each stomata individually and the mean value of each feature was subsequently calculated. The features included in the dataset were: convex area [30], contour area [30], perimeter, solidity [30], elongation [11], circularity [11], object width and object height.

ICCS Camera Ready Version 2025
To cite this paper please use the final published version:
DOI: 10.1007/978-3-031-97564-6_11

The classical machine learning algorithms selected for this analysis were K-Nearest Neighbors (KNN) [18], Random Forest (RF) [20], Support Vector Machine (SVM) [22] and Multi-Layer Perceptron [1]. The hyperparameters of these models were tuned to optimize performance. Specifically: for KNN, the number of neighbors k was varied from 1 to 10; in RF, the number of trees was tested from 100 to 500; the regularization parameter C in SVM was evaluated over the range from 0.8 to 2.6. The architecture of the MLP was explored using configurations with three hidden layers, ranging from $10\times10\times10$ neurons to $20\times20\times20$ neurons. All experiments were conducted using 10-fold cross-validation to ensure the robustness and reliability of the results.

The computations were conducted on the *Image masks* and *Subimage masks* with and without the application of majority voting. The highest accuracy results, corresponding to the evaluated parameter values, are summarized in Table 2. Although MV generally enhances classification accuracy compared to the performance on the *Subimage masks* dataset without MV, it only improves the classification accuracy of whole images in the case of MLP (0.627 with MV on *Subimage masks* vs. 0.548 on *Image masks*). For the other methods, classification on *Image masks* dataset yields higher accuracy compared to its application to *Subimage masks* both with and without MV. Among classical machine learning methods, the highest accuracy obtained on binary masks is achieved with Random Forest, reaching 0.758. However, this is lower than the accuracy obtained on binary masks with deep learning, where ResNet50v2 without MV achieved 0.787, outperforming the classical approaches.

	Image masks		***Subimage masks***		***Subimage masks* MV**	
method	**ACC**	***adj. param.***	**ACC**	***adj. param.***	**ACC**	***adj. param.***
KNN	0.706	$k = 2$	0.63	$k = 10$	0.643	$k = 10$
SVM	0.647	$C = 1.8$	0.62	$C = 2.6$	0.569	$C = 2.4$
RF	0.758	$n = 400$	0.646	$n = 350$	0.692	$n = 300$
MLP	0.548	$14 \times 14 \times 14$	0.585	$16 \times 16 \times 16$	0.627	$14 \times 14 \times 14$

Table 2: The highest classification accuracy for stomata images on the *Image masks* and *Subimage masks* datasets achieved using classical machine learning methods, with or without the application of majority voting, across the evaluated set of adjusted hyperparameters (*adj. param.*).

5 Conclusions and discussion

The application of deep learning for dataset classification demonstrated remarkable accuracy, reaching values as high as 0.973 for *Images* dataset with ResNet152v2. It is important to emphasize that the classes under analysis exhibited distinct color variations. This characteristic may lead the model to make overly optimistic predictions, resulting in inflated accuracy metrics.

ICCS Camera Ready Version 2025
To cite this paper please use the final published version:
DOI: 10.1007/978-3-031-97564-6_11

To investigate the extent to which color influences classification performance, the dataset was transformed into other color spaces designed to minimize inter-class color variation. This approach aimed to challenge the model's reliance on color-based features. Consequently, the classification accuracy notably decreased, with ResNet50v2 achieving a reduced accuracy of just 0.606 on *HSV images - H* dataset. These findings underscore the importance of evaluating model performance under varying color conditions to ensure robust and generalizable classification results.

To further refine the analysis, the focus was narrowed to stomata objects by extracting subimages containing individual stomata instances. In most cases, this approach resulted in decreased classification accuracy compared to using whole images. For instance, while ResNet50v2 achieved an accuracy of 0.953 on the *Image* dataset, the accuracy dropped to 0.856 when applied to the *Subimages*.

To enhance performance on subimages, a majority voting approach was implemented, which involved aggregating predictions from multiple subimages. This strategy generally led to improved accuracy compared to classifying individual subimages alone. However, despite the gains, the MV approach did not outperform classification on whole images. For instance, *Subimages* with ResNet50v2 and MV achieved an accuracy of 0.913, which remained lower than the 0.953 accuracy obtained with the *Image*.

To eliminate the influence of color entirely, the analysis was conducted on image masks, which preserve only the shape of the stomata. On the *Image masks* dataset, classification accuracy was 0.787 and 0.68 using ResNet50v2 and ResNet152v2, respectively. Further experimentation involved applying the same approach to *Subimage masks*, focusing on individual stomata objects. In this scenario, the highest accuracy achieved was 0.624 using ResNet152v2 with the majority voting strategy. These results highlight a noticeable decrease in performance compared to color images, emphasizing the significant role color plays in model accuracy and the challenges of relying solely on structural features for classification.

The classification results obtained using deep learning on mask datasets were compared with those achieved using a classical approach based on handcrafted shape features. After hyperparameter optimization, the highest accuracy for *Image masks* was 0.758 using Random Forest, while for *Subimage masks*, the best result was 0.692, also with Random Forest combined with majority voting. These results demonstrate that better outcomes are achieved when the entire mask is classified, as not only the shape of the stomata is important, but also the dependencies between different objects and their spatial arrangement in the image.

Deep learning models outperformed the classical approach when applied to *Image masks* containing multiple stomata instances, achieving an accuracy of 0.787 with ResNet50v2 compared to 0.758 with Random Forest on the same dataset. However, when focused on *Subimage masks*, ResNet models were outperformed by handcrafted shape features combined with majority voting. Specifically, ResNet152v2 with majority voting achieved an accuracy of 0.624, whereas Random Forest with majority voting reached 0.692. These results suggest that

ICCS Camera Ready Version 2025
To cite this paper please use the final published version:
DOI: 10.1007/978-3-031-97564-6_11

deep learning effectively utilizes spatial context, while handcrafted features are more effective when spatial dependencies are absent.

These findings underscore the importance of considering environmental factors in ploidy classification. A key challenge for researchers is to avoid relying on color-related features, as subtle differences in leaf shade can lead to inflated classification accuracy. The studied cultivars differed in ripening time. For instance, 'Gofert' is an early ripening variety - the fruit ripens in the first decade of July, while 'Polares' ripens in the last decade of July, which can influence the condition of the leaves collected at the end of the vegetation season.

This preliminary research highlights the need to prepare datasets under diverse conditions to introduce greater variation in stomata size and leaf color within each class. By doing so, the resulting models will be more robust to environmental variations, ensuring more reliable and generalizable classification outcomes. In addition, maintaining uniform conditions for plant growth may facilitate visual differentiation between classes by scientists. However, this consistency can lead models to learn spurious correlations that should not be the basis for classification. Therefore, to achieve reliable and meaningful results, it is crucial to design datasets that challenge the model to focus on essential biological features rather than environmental cues.

6 Acknowledgements

The authors are grateful to Prof. Stanisław Pluta and Prof. Małgorzata Podwyszyńska for providing access to the plant materials used in the experiments.

References

1. Alsmadi, M.k., Omar, K.B., Noah, S.A., Almarashdah, I.: Performance comparison of Multi-layer Perceptron (Back Propagation, delta rule and Perceptron) algorithms in neural networks. In: 2009 IEEE International Advance Computing Conference. p. 296–299. IEEE (2009). https://doi.org/10.1109/iadcc.2009.4809024
2. Anli, M., Boutasknit, A., Ait-El-Mokhtar, M., Ben-Laouane, R., Ait-Rahou, Y., Fakhech, A., Meddich, A.: Improving lettuce yield and quality of an agricultural soil using a combination of arbuscular mycorrhizal fungus and phosphate-green wastes compost. Gesunde Pflanzen **74**(1), 205–217 (2021). https://doi.org/10.1007/s10343-021-00603-0
3. Avaneesh, J., Thangakumar, J., Sudalaimuthu, T., Ranjana, P., Prakash, N.S., Teja, N.S.: Accurate object detection with YOLO. International Journal of Pharmaceutical Research **12**(01) (2020). https://doi.org/10.31838/ijpr/2020.12.01.235
4. Balakrishnan, D., Manideep Kumar Reddy, S., Lakshmi Venkatesh, R., Aadith, K., Jebi Nalatharaj, R., Arshath, M.: Object detection on traffic data using YOLO. In: 2023 International Conference on Data Science and Network Security (ICDSNS). p. 1–5. IEEE (2023). https://doi.org/10.1109/icdsns58469.2023.10245691
5. Casson, S.A., Hetherington, A.M.: Environmental regulation of stomatal development. Current Opinion in Plant Biology **13**(1), 90–95 (2010). https://doi.org/10.1016/j.pbi.2009.08.005

ICCS Camera Ready Version 2025
To cite this paper please use the final published version:
DOI: 10.1007/978-3-031-97564-6_11

6. Chua, L.C., Lau, O.S.: Stomatal development in the changing climate. Development **151**(20) (2024). https://doi.org/10.1242/dev.202681
7. Deng, T.: A survey of Convolutional Neural Networks for image classification: Models and datasets. In: 2022 International Conference on Big Data, Information and Computer Network (BDICN). p. 746–749. IEEE (2022). https://doi.org/10.1109/bdicn55575.2022.00145
8. Farag, M.M.: Design and analysis of Convolutional Neural Layers: A signal processing perspective. IEEE Access **11**, 27641–27661 (2023). https://doi.org/10.1109/access.2023.3258399
9. Fetter, K.C., Eberhardt, S., Barclay, R.S., Wing, S., Keller, S.R.: Stomatacounter: a neural network for automatic stomata identification and counting. New Phytologist **223**(3), 1671–1681 (2019). https://doi.org/10.1111/nph.15892
10. Ghosh, A., Sufian, A., Sultana, F., Chakrabarti, A., De, D.: Fundamental Concepts of Convolutional Neural Network, p. 519–567. Springer International Publishing (2019). https://doi.org/10.1007/978-3-030-32644-9_36
11. Guan, H., Antani, S., Long, L.R., Thoma, G.R.: Comparative study of spine vertebra shape retrieval using learning-based feature selection. In: 2009 22nd IEEE International Symposium on Computer-Based Medical Systems. p. 1–7. IEEE (2009). https://doi.org/10.1109/cbms.2009.5255384
12. He, K., Zhang, X., Ren, S., Sun, J.: Deep Residual Learning for image recognition. In: 2016 IEEE Conference on Computer Vision and Pattern Recognition (CVPR). IEEE (2016). https://doi.org/10.1109/cvpr.2016.90
13. He, K., Zhang, X., Ren, S., Sun, J.: Identity mappings in Deep Residual Networks (2016). https://doi.org/10.48550/ARXIV.1603.05027
14. Jocher, G., Chaurasia, A., Qiu, J.: Ultralytics YOLOv8 (2023), https://github.com/ultralytics/ultralytics
15. Kaur, S., Agrawal, R.: Convolutional Networks (2021). https://doi.org/10.1002/9781119760542.ch8
16. Konopka, A., Kozera, R., Sas-Paszt, L., Trzcinski, P., Lisek, A.: Identification of the selected soil bacteria genera based on their geometric and dispersion features. PLOS ONE **18**(10), e0293362 (2023). https://doi.org/10.1371/journal.pone.0293362
17. Konopka, A., Struniawski, K., Kozera, R.: Performance analysis of Residual Neural Networks in soil bacteria microscopic image classification. In: 37th Annual European Simulation and Modelling Conference, ESM 2023. pp. 144–148 (2023)
18. Konopka, A., Struniawski, K., Kozera, R., Trzciński, P., Sas-Paszt, L., Lisek, A., Górnik, K., Derkowska, E., Głuszek, S., Sumorok, B., Frąc, M.: Classification of soil bacteria based on machine learning and image processing. In: International Conference on Computational Science – ICCS 2022. pp. 263–277. Springer International Publishing (2022). https://doi.org/10.1007/978-3-031-08757-8_23
19. Ku, K.B., Le, A.T., Thai, T.T., Mansoor, S., Kittipadakul, P., Duangjit, J., Kang, H.M., Oh, S.S.M., Phan, N.H., Chung, Y.S.: New dimension in leaf stomatal behavior analysis: a robust method with machine learning approach. Plant Biotechnology Reports **18**(3), 361–373 (2024). https://doi.org/10.1007/s11816-024-00902-8
20. Liu, Y., Wang, Y., Zhang, J.: New Machine Learning Algorithm: Random Forest, p. 246–252. Springer Berlin Heidelberg (2012). https://doi.org/10.1007/978-3-642-34062-8_32
21. Ma, Y., Zhao, F., Wang, L., Ding, Y., Zhao, H., Wang, H., Liu, J.: A stomata-inspired superhydrophobic portable filter system. RSC Advances **11**(31), 18783–18786 (2021). https://doi.org/10.1039/d1ra03297f

ICCS Camera Ready Version 2025
To cite this paper please use the final published version:
DOI: 10.1007/978-3-031-97564-6_11

22. Mammone, A., Turchi, M., Cristianini, N.: Support vector machines. WIREs Computational Statistics **1**(3), 283–289 (2009). https://doi.org/10.1002/wics.49
23. Podwyszyńska, M., Pluta, S.: In vitro tetraploid induction of the blackcurrant (ribes nigrum l.) and preliminary phenotypic observations. Zemdirbyste-Agriculture **106**(2), 151–158 (2019). https://doi.org/10.13080/z-a.2019.106.020
24. Prakash, I.V., Palanivelan, M.: A Study of YOLO (You Only Look Once) to YOLOv8, p. 257–266. CRC Press (2024). https://doi.org/10.1201/9781003529231-40
25. Rothe, R., Guillaumin, M., Van Gool, L.: Non-maximum Suppression for Object Detection by Passing Messages Between Windows, p. 290–306. Springer International Publishing (2015). https://doi.org/10.1007/978-3-319-16865-4_19
26. Sabba, S., Smara, M., Benhacine, M., Terra, L., Eddine Terra, Z.: Residual Neural Network in genomics. Computer Science Journal of Moldova **30**(3(90)), 308–334 (2022). https://doi.org/10.56415/csjm.v30.17
27. Sai, N., Bockman, J.P., Chen, H., Watson-Haigh, N., Xu, B., Feng, X., Piechatzek, A., Shen, C., Gilliham, M.: Stomaai: an efficient and user-friendly tool for measurement of stomatal pores and density using deep computer vision. New Phytologist **238**(2), 904–915 (2023). https://doi.org/10.1111/nph.18765
28. Shen, Z., Liu, Y.: A novel connectivity of deep Convolutional Neural Networks. In: 2017 Chinese Automation Congress (CAC). p. 7779–7783. IEEE (2017). https://doi.org/10.1109/cac.2017.8244187
29. Struniawski, K., Konopka, A., Kozera, R.: Identification of soil bacteria with machine learning and image processing techniques applying single cells' region isolation. In: The European Simulation and Modelling Conference 2022. pp. 76–81. EUROSIS-ETI (2022)
30. Wang, X., Zhang, J.: An improved automatic shape feature extraction method based on template matching. Journal of Physics: Conference Series **2095**(1), 012053 (2021). https://doi.org/10.1088/1742-6596/2095/1/012053
31. Ye, J.C.: Convolutional Neural Networks, p. 113–134. Springer Nature Singapore (2021). https://doi.org/10.1007/978-981-16-6046-7_7
32. Zeiditoolabi, N., Khammari, I., Sirousmehr, A., Daneshvar, M., Galavi, M., Dahmardeh, M.: Evaluation of stomata in vetch-barley intercropping and its relationship with forage production in rainfed conditions, under the influence of biofertilizer and superabsorbent. Gesunde Pflanzen **75**(5), 2045–2073 (2023). https://doi.org/10.1007/s10343-023-00838-z
33. Zhao, L., Zhang, Z.: A improved pooling method for Convolutional Neural Networks. Scientific Reports **14**(1) (2024). https://doi.org/10.1038/s41598-024-51258-6
34. Zulunov, R., Soliyev, B., Kayumov, A., Asraev, M., Musayev, K., Abdurasulova, D.: Detecting mobile objects with AI using edge detection and background subtraction techniques. E3S Web of Conferences **508**, 03004 (2024). https://doi.org/10.1051/e3sconf/202450803004
35. Šmarda, P., Klem, K., Knápek, O., Veselá, B., Veselá, K., Holub, P., Kuchař, V., Šilerová, A., Horová, L., Bureš, P.: Growth, physiology, and stomatal parameters of plant polyploids grown under ice age, present day, and future CO2 concentrations. New Phytologist **239**(1), 399–414 (2023). https://doi.org/10.1111/nph.18955

ICCS Camera Ready Version 2025
To cite this paper please use the final published version:
DOI: 10.1007/978-3-031-97564-6_11